

AN X-RAY + RADIO SEARCH FOR MASSIVE BLACK HOLES IN BLUE COMPACT DWARF GALAXIES

LILIKOI J. LATIMER

eXtreme Gravity Institute, Department of Physics, Montana State University, Bozeman, MT 59717, USA

AMY E. REINES

eXtreme Gravity Institute, Department of Physics, Montana State University, Bozeman, MT 59717, USA

RICHARD M. PLOTKIN

International Centre for Radio Astronomy Research, Curtin University, GPO Box U1987, Perth, WA 6845, Australia and
Department of Physics, University of Nevada, Reno, NV 89557, USA

THOMAS D. RUSSELL

Anton Pannekoek Institute for Astronomy, University of Amsterdam, Science Park 904, 1098 XH, Amsterdam, The Netherlands

AND

JAMES J. CONDON

National Radio Astronomy Observatory, Charlottesville, VA 22903, USA

Draft version June 24, 2022

ABSTRACT

Nearby blue compact dwarf (BCD) galaxies are arguably our best local analogues of galaxies in the earlier Universe that may host relics of black hole (BH) seeds. Here we present high-resolution *Chandra X-ray Observatory* and Karl G. Jansky Very Large Array (VLA) observations of five nearby BCDs with stellar masses of less than the Small Magellanic Cloud ($M_* \sim 10^7 - 10^{8.4} M_\odot$). We search for signatures of accreting massive BHs at X-ray and radio wavelengths, which are more sensitive to lower BH accretion rates than optical searches. We detect a total of 10 hard X-ray sources and 10 compact radio sources at luminosities consistent with star-formation-related emission. We find one case of a spatially-coincident X-ray and radio source within the astrometric uncertainties. If the X-ray and radio emission are indeed coming from the same source, the origin of the radiation is plausibly from an active massive BH with $\log(M_{\text{BH}}/M_\odot) \sim 4.8 \pm 1.1$. However, given that the X-ray and radio emission are also coincident with a young star cluster complex, we consider the combination of an X-ray binary and a supernova remnant (or H II region) a viable alternative explanation. Overall, we do not find compelling evidence for active massive BHs in our target BCDs, which on average have stellar masses more than an order of magnitude lower than previous samples of dwarf galaxies found to host massive BHs. Our results suggest that moderately accreting massive BHs in BCDs are not so common as to permit unambiguous detection in a small sample.

Keywords: galaxies: active — galaxies: dwarf — galaxies: nuclei — X-rays: galaxies — radio continuum: galaxies

1. INTRODUCTION

Over the past several years there has been mounting evidence for the existence of massive black holes (BHs) in at least some dwarf galaxies (e.g., Reines et al. 2011, 2013, 2014; Baldassare et al. 2015, 2016, 2017; Baldassare et al. 2018; Schramm et al. 2013; Moran et al. 2014; Lemons et al. 2015; Hainline et al. 2016; Pardo et al. 2016; Dickey et al. 2019; Nguyen et al. 2019). This has important implications for the formation and growth of the first “seeds” of supermassive black holes that are ubiquitous in today’s massive galaxies (e.g., Kormendy & Richstone 1995; Kormendy & Ho 2013). For example, present-day BH-host galaxy scaling relations at low masses and the BH occupation fraction in dwarf galaxies are predicted to be strong discriminants between seeds that were heavy ($\sim 10^5 M_\odot$) or light ($\sim 10^2 M_\odot$) (e.g., Volonteri 2010; Greene 2012; Ricarte & Natarajan 2018).

While there has been recent progress on the observational front, the BH occupation fraction in dwarf galaxies is not yet well determined (although see Miller et al. 2015) and we know very little about the types of dwarf galaxies that may be preferential hosts to massive BHs. Dwarf galaxies come in a variety of flavors, including star-forming irregulars, spirals and blue compact dwarfs, early-type ellipticals and ultracompact dwarfs, and dark-matter-dominated dwarf spheroidals and ultrafaint dwarfs. So far the largest samples of massive BHs in dwarf galaxies have been found by applying optical emission line diagnostics (e.g., BPT selection and broad H α ; Reines et al. 2013) to Sloan Digital Sky Survey (SDSS) spectroscopy. However, these types of optical searches are biased towards active BHs that are more easily observed, such as those with high Eddington ratios and those that are unobscured by star formation. Indeed, the host galaxies of the Reines et al. (2013) sample tend to have bright nuclear point sources (from the active galac-

tic nuclei, i.e., AGN), regular morphologies, and little ongoing star formation (Schutte et al., in prep; Kimbrell et al., in prep). This is similar to the slightly more massive counterparts in the earlier sample of Greene & Ho (2007).

Given that our understanding of the demographics of massive BHs in different categories of dwarf galaxies is quite limited, and the surprising discovery of a massive BH in the blue compact dwarf (BCD) galaxy Henize 2-10 (Reines et al. 2011), we have observed a small sample of BCDs using X-ray and radio observations. High-resolution observations from the *Chandra X-ray Observatory* and the Very Large Array (VLA) are especially well-suited to searching for weakly accreting massive BHs and those residing in star-forming host galaxies, as exemplified by detailed studies of Henize 2-10 (Reines et al. 2011; Reines & Deller 2012; Reines et al. 2016) that reveal a spatially coincident compact, non-thermal radio and X-ray point source at the center of the galaxy.¹ Moreover, BCDs are characterized by blue colors, low metallicities, and concentrated regions of intense star formation (e.g. Gil de Paz et al. 2003), making them our best local analogues of low-mass, physically small, gas-rich, star-forming galaxies in the earlier Universe, where the first BH seeds likely formed.

2. SAMPLE OF BLUE COMPACT DWARF GALAXIES

Our target galaxies are taken from the sample of BCDs from Gil de Paz et al. (2003). Gil de Paz et al. (2003) propose that a galaxy must fulfill the following observational criteria in order to be classified as a BCD: (1) blue with $\mu_{B,\text{peak}} - \mu_{R,\text{peak}} \lesssim 1 \text{ mag arcsec}^{-2}$, (2) compact with $\mu_{B,\text{peak}} < 22 \text{ mag arcsec}^{-2}$, and (3) a dwarf with $M_K > -21 \text{ mag}$. This definition separates the BCDs from other types of dwarf galaxies such as dwarf irregulars and dwarf ellipticals. Given that our search technique depends on high-resolution X-ray and radio observations, we adopted two complementary strategies for selecting our target BCDs from Gil de Paz et al. (2003).

First, we selected galaxies detected at 1.4 GHz in the Faint Images of the Radio Sky at Twenty-cm (FIRST) survey (Becker et al. 1995) with distances $< 20 \text{ Mpc}$. BCDs detected by FIRST are preferred targets since they must either have an AGN and/or intense star formation to produce the observed radio emission on scales of $\sim 5''$, making them good analogues of Henize 2-10. The distance cut was applied to retain both sensitivity to low luminosities and fine enough spatial resolution to accurately determine if X-ray and radio sources are co-incident. Out of the 80 BCDs in Gil de Paz et al. (2003) covered by the FIRST survey area, four galaxies met these selection criteria: Haro 3, Haro 9, Mrk 709² and II Zw 70. These four BCDs were the subject of a joint *Chandra*-VLA proposal (PI: Reines; CXO proposal number 13700563, VLA project SD0563). Our study of Mrk 709, and its candidate massive BH, has previously

¹ Although see Hebbard et al. (2019) who argue for a supernova remnant origin. We defer a detailed discussion of this object to a forthcoming paper.

² The distance of 15.7 Mpc for Mrk 709 provided in Gil de Paz et al. (2003) (from NED) was incorrect. Reines et al. (2014) present a redshift of $z = 0.052$ ($d \sim 214 \text{ Mpc}$) based on SDSS spectroscopy.

been presented in Reines et al. (2014).

To expand our sample, we also searched for BCDs in the sample of Gil de Paz et al. (2003) with available observations in the *Chandra* archive. We found 18 galaxies with *Chandra* coverage and, after obtaining and inspecting these data, found five BCDs with detectable hard X-ray point sources worthy of radio follow-up with the VLA (any existing VLA archival data were not deep enough and/or lacked sufficient resolution to meet our requirements). We proposed for VLA observations of these preferred targets with existing X-ray sources, however only two (Mrk 996 and SBS 0940+544) were ultimately observed for this project (PI Reines; VLA project 12B-206) due to scheduling priorities. We did not propose for the remaining 13 galaxies without detectable *Chandra* point sources since we are primarily interested in finding spatially coincident X-ray and radio sources as a signpost of massive BH accretion.

Our final sample consists of five BCD galaxies (see Figure 1) and their properties are given in Table 1. Note that while distances from Gil de Paz et al. (2003) were used to initially select our sample, in our analysis here we use distances derived from redshifts in the NASA-Sloan Atlas³ (NSA) with $h = 0.73$.

3. OBSERVATIONS AND DATA REDUCTION

3.1. *Chandra X-ray Observatory*

X-ray observations of our target galaxies were taken with *Chandra* between 2009 Sep 03 and 2012 Dec 31. Exposure times were between 16.8 ks and 53.3 ks. A summary of the *Chandra* X-ray observations is given in Table 2.

Each dwarf galaxy was placed at the aimpoint of the ACIS S3 chip. We used the *Chandra* Interactive Analysis of Observations (CIAO) software v4.7 (Fruscione et al. 2006) to reduce each observation. We first reprocessed the data by applying calibration files (CALDB 4.6.7), and we determined that no observations were affected by background flares.

We then aligned each *Chandra* observation to the optical SDSS astrometric frame, using the CIAO tool `reproject_aspect`. To align the astrometry, we created a list of X-ray point sources on the S3 chip by running the point source detection algorithm `wavdetect` on a *Chandra* image filtered from 0.5-7 keV. We then excluded all X-ray sources falling within $3r_{50}$ of the dwarf galaxy, and we correlated the remaining X-ray sources to optical point sources in the SDSS DR12 with $i < 22 \text{ mag}$. We found 2-5 common X-ray and optical point sources on the S3 chip for each observation. Given the small number of common sources, we only applied a translation correction to the *Chandra* images in the x,y directions. The applied astrometric shifts range from ± 0.01 -1.3 pixels, and the median shifts across all five observations were $|\Delta x| = 0.2$ and $|\Delta y| = 0.4$ pixels ($0''.1$ and $0''.2$, respectively).

3.2. *Karl G. Jansky Very Large Array*

Observations of our sample of galaxies were taken with the VLA in its extended A-configuration between 2012 December 1 and 2013 January 1. The observations typically provided between 50 minutes and 90 minutes of on

³ <http://nsatlas.org>, version 0.1.2

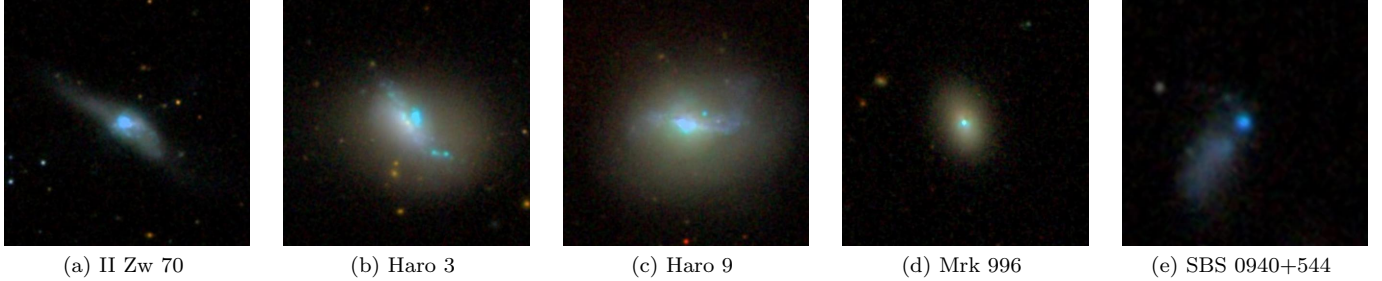


Figure 1. SDSS color composite images of the galaxies in our sample. Each image has dimensions of $1.69' \times 1.69'$, except for (e), which has dimensions of $0'.85 \times 0'.85$.

Table 1
Sample of Blue Compact Dwarf Galaxies

Galaxy	R.A.	Decl.	N_{H} (10^{20} cm^{-2})	z	r_{50} (kpc)	Distance (Mpc)	M_g (mag)	$g - i$ (mag)	$\log M_*/M_{\odot}$
(1)	(2)	(3)	(4)	(5)	(6)	(7)	(8)	(9)	(10)
II Zw 70	14 50 56.5	+35 34 18	1.16	0.00470	0.30	19.31	-16.98	-0.289	7.28
Haro 3	10 45 22.4	+55 57 37	0.66	0.00409	0.61	16.81	-18.21	-0.062	8.03
Haro 9	12 45 17.1	+27 07 32	0.71	0.00443	0.84	18.18	-18.92	0.103	8.38
Mrk 996	01 27 35.5	-06 19 36	3.83	0.00491	0.46	20.18	-17.38	0.081	7.73
SBS 0940+544	09 44 16.6	+54 11 34	1.34	0.00652	0.83	26.78	-15.97	-0.256	7.04

Note. — Column 1: galaxy name. Column 2: right ascension in units of hours, minutes, seconds (J2000). Column 3: declination in units of degrees, arcminutes, arcseconds (J2000). Column 4: galactic neutral hydrogen column density. Column 5: redshift, specifically the `zdist` parameter from the NSA. Column 6: Petrosian 50% light radius. Column 7: distance estimate from `zdist`. Column 8: absolute g -band magnitude corrected for foreground Galactic extinction. Column 9: $g - i$ color. Column 10: \log galaxy stellar mass. The values given in columns 5-10 are from the NSA^a and we assume $h = 0.73$.

^aSBS 0940+544 appears as two separate sources in the NSA; one for the bright central region, and one for the trailing tail region (see Figure 1). The values for M_g , $g - i$ color, and $\log M_*$ (Columns 8, 9, and 10) are from the combined sources, while the values for z , r_{50} , and distance (Columns 5, 6, and 7) are from the bright central region (though the trailing tail region has similar values).

Table 2
Chandra Observations

Galaxy	Date observed	Obs ID	Exp. time (ks)	$N_{\text{background}}$
II Zw 70	2011 Nov 06	13930	30.6	0.033
Haro 3	2012 Dec 31	13927	17.8	0.131
Haro 9	2012 Nov 13	13928	16.8	0.176
Mrk 996	2009 Sep 03	11567	53.3	0.104
SBS 0940+544	2010 Jan 18	11288	16.8	0.079

Note. — $N_{\text{background}}$ is the number of expected 2-10 keV $N(> S)$ background sources within $3r_{50}$, using Moretti et al. (2003).

source time (see Table 3). All observations were taken at C -band with two 1-GHz wide basebands centered at 5.0 and 7.4 GHz, each comprised of eight 128-MHz subbands containing 64 spectral channels of width 2-MHz. The primary (bandpass and amplitude) and secondary (phase) calibrators are given in Table 3.

The data were edited and calibrated following standard procedures within the Common Astronomy Software Application (CASA; McMullin et al. 2007). Using natural weighting for maximum sensitivity, we imaged the calibrated data separately at 5.0 and 7.4 GHz (Figure 2), where deconvolution (cleaning) was carried out with the multi-frequency synthesis algorithm within CASA. The RMS noise and beam parameters are given for each image in Table 4. We also explored different antenna weightings, and used UV-cuts to filter out diffuse emission (as well as match spatial sensitivity between the 5.0 and 7.4 GHz images). However, these did not alter the results,

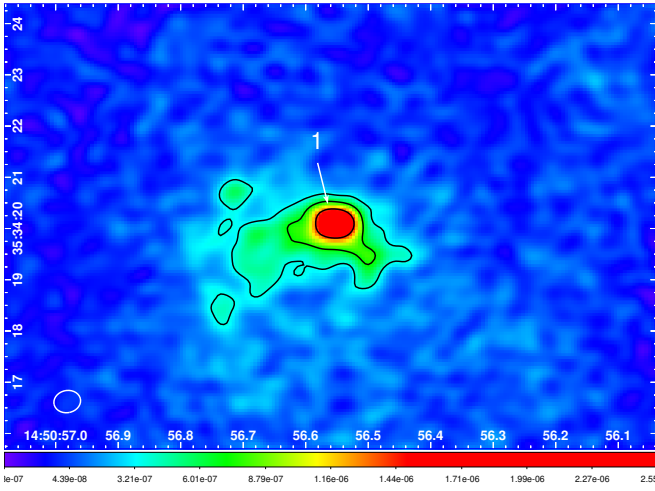
and, therefore, we only present the images using natural weighting to maximize the sensitivity. The absolute astrometry of the VLA observations is accurate to $\lesssim 0'.1$.

3.3. Optical Images

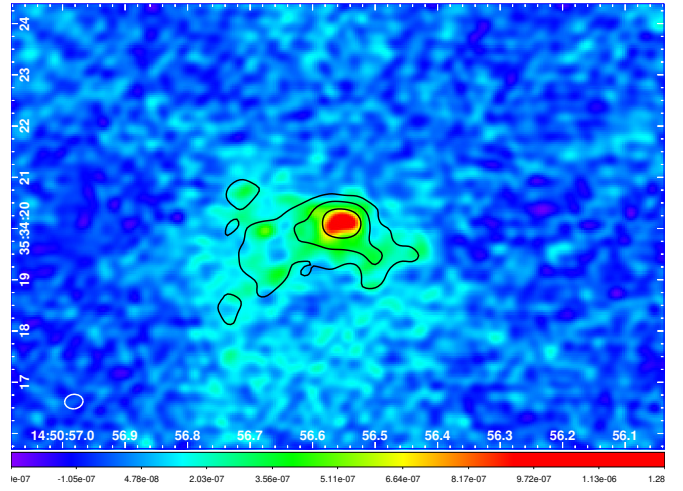
We obtained optical images of our target galaxies for comparison with the X-ray and radio observations. SDSS color composite images of the BCDs are shown in Figure 1. We also retrieved archival *Hubble Space Telescope* (*HST*) WFPC2 broadband images of three galaxies (Haro 3, Haro 9, and Mrk 996) from the Hubble Legacy Archive. The absolute astrometry of the *HST* images was adjusted to match the SDSS using common sources in each image. The astrometric corrections were $\lesssim 0'.2$.

4. ANALYSIS AND RESULTS

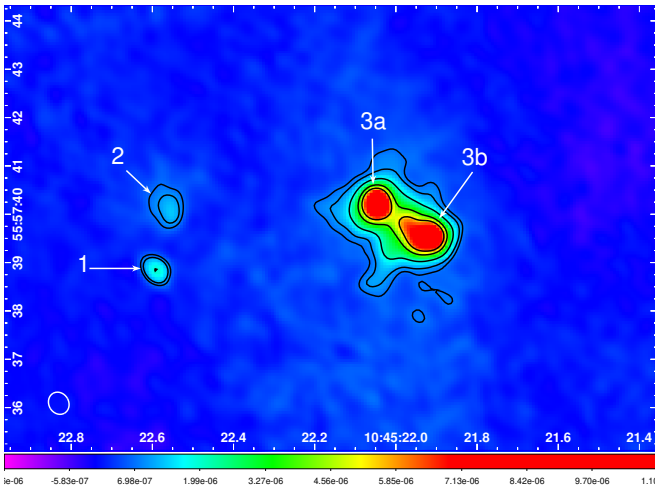
4.1. Host Galaxies and Star Formation Rates



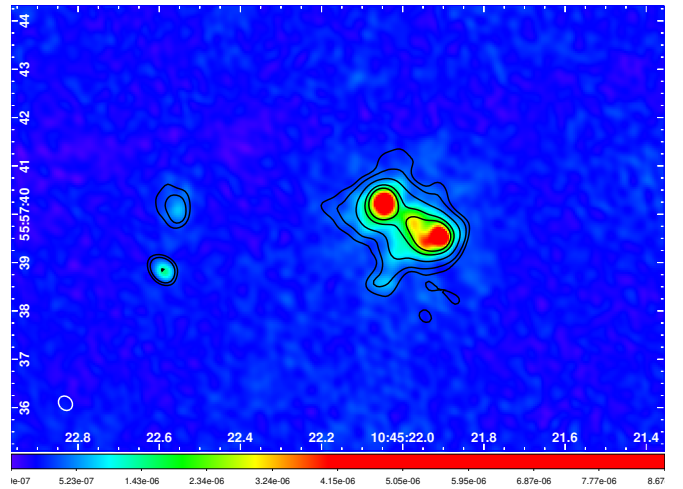
(a) II Zw 70 VLA 5 GHz image with contour levels of $(\sqrt{2})^n$ times the RMS noise, where $n = 5, 7,$ and 9 .



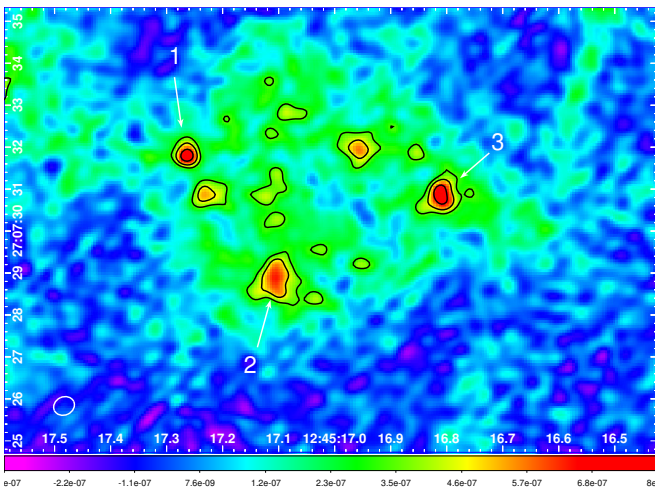
(b) II Zw 70 VLA 7.4 GHz image with the 5 GHz contour levels overlaid.



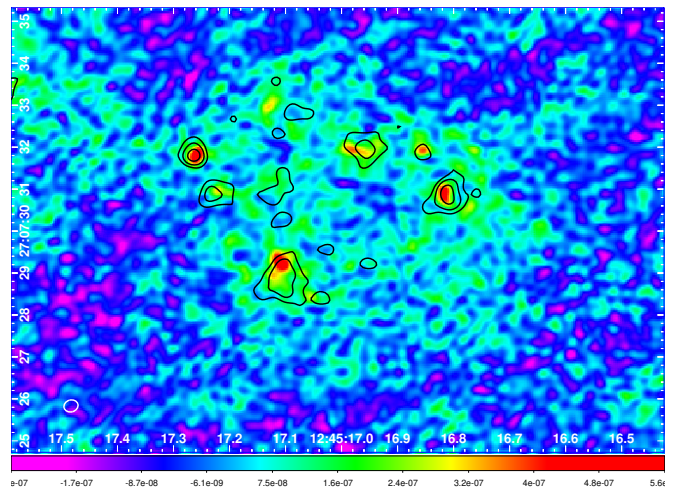
(c) Haro 3 VLA 5 GHz image with contour levels of $(\sqrt{2})^n$ times the RMS noise, where $n = 4, 5, 7, 9,$ and 10 .



(d) Haro 3 VLA 7.4 GHz image with the 5 GHz contour levels overlaid..



(e) Haro 9 VLA 5 GHz image with contour levels of $(\sqrt{2})^n$ times the RMS noise, where $n = 4, 5,$ and 6 .



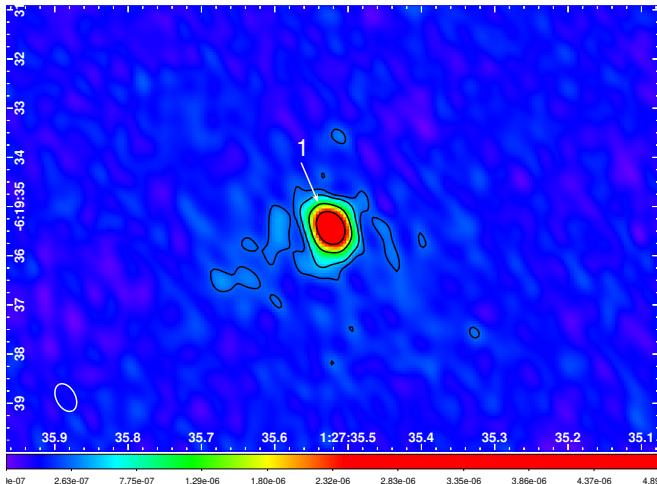
(f) Haro 9 VLA 7.4 GHz image with the 5 GHz contour levels overlaid.

Figure 2. VLA 5 GHz (left) and 7.4 GHz (right) images of the galaxies in our sample. The beam sizes are shown in the lower left corners.

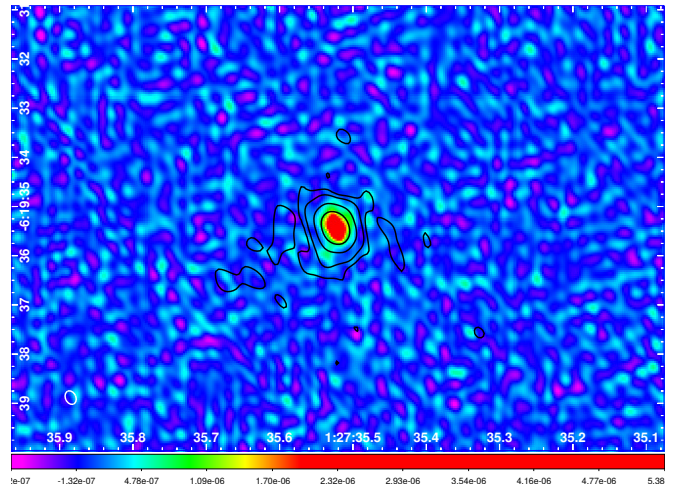
Table 3
VLA Observations

Galaxy	Date Observed	Project Code	Flux Calibrator	Phase Calibrator	Time on Source (min)
II Zw 70	2012 Dec 01	SD0563	3C 286	J1416+3444	90
Haro 3	2012 Dec 02	SD0563	3C 286	J1035+5628	50
Haro 9	2012 Dec 01	SD0563	3C 286	J1221+2813	80
Mrk 996	2013 Jan 01	12B-206	3C 48	J0110-0741	90
SBS 0940+544	2012 Dec 24	12B-206	3C 147	J0932+5306	50

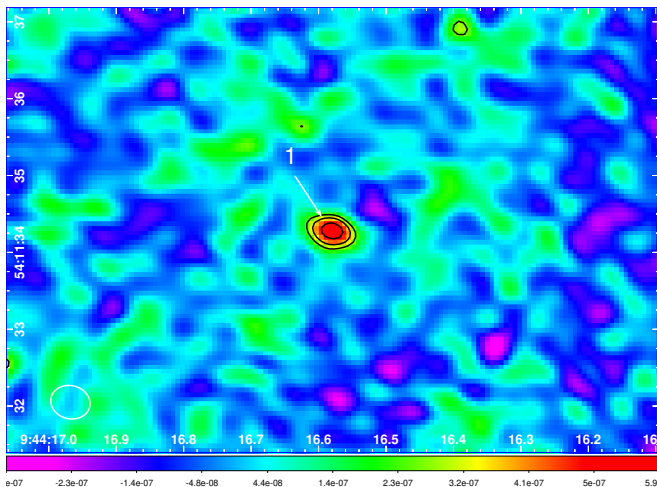
Note. — All observations were taken at *C*-band while the VLA was in the A-configuration.



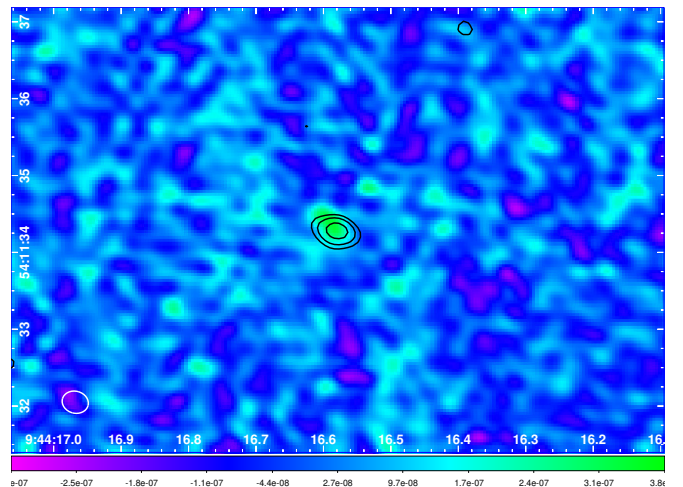
(g) Mrk 996 VLA 5 GHz image with contour levels of $(\sqrt{2})^n$ times the RMS noise, where $n = 3, 5, 8,$ and 10 .



(h) Mrk 996 VLA 7.4 GHz image with the 5 GHz contour levels overlaid.



(i) SBS 0940+544 VLA 5 GHz image with contour levels of $(\sqrt{2})^n$ times the RMS noise, where $n = 4, 5,$ and 6 .



(j) SBS 0940+544 VLA 7.4 GHz image with the 5 GHz contour levels overlaid.

Figure 2. VLA 5 GHz (left) and 7.4 GHz (right) images of the galaxies in our sample. The beam sizes are shown in the lower left corners.

Table 4
Imaging Parameters for VLA Observations

Galaxy (1)	ν (GHz) (2)	Synthesized Beam (arcsec) (3)	P.A. (deg) (4)	rms Noise (μ Jy beam $^{-1}$) (5)
II Zw 70	5.0	0.52×0.43	-78.7	4.5
...	7.4	0.36×0.28	-83.0	4.3
Haro 3	5.0	0.47×0.41	30.2	10.4
...	7.4	0.32×0.27	40.5	5.7
Haro 9	5.0	0.51×0.43	-65.1	5.6
...	7.4	0.34×0.28	-74.2	4.4
Mrk 996	5.0	0.60×0.39	27.9	4.6
...	7.4	0.29×0.21	25.2	7.6
SBS 0940+544	5.0	0.52×0.43	75.9	5.9
...	7.4	0.35×0.29	75.1	5.2

Note. — Column 1: galaxy name. Column 2: rest frequency. Column 3: beam major axis \times beam minor axis. Column 4: beam position angle. Column 5: RMS noise of the image. All images were produced using natural weighting for maximum sensitivity.

The five galaxies in our sample (see Figure 1) span a stellar mass range of $\sim 10^7 - 10^{8.4} M_{\odot}$, with a median of $\sim 10^8 M_{\odot}$. It is worth noting that these galaxies have more irregular morphologies and significantly lower stellar masses than previous samples of dwarf galaxies found to host AGNs (e.g., Reines et al. 2013). The galaxies are also physically small, with half-light radii less than 1 kpc. All of the galaxies are relatively nearby, with distances in the range of ~ 17 -27 Mpc (using the `zdist` parameter in the NSA and adopting $h_0 = 0.73$). See Table 1 for information on the individual galaxies.

In general, BCDs are experiencing regions of intense star formation. We estimate the star formation rates (SFRs) of our target BCD galaxies using far-UV (FUV; 1528 Å) and mid-infrared (IR; 25 μ m) luminosities via

$$\begin{aligned} \log \text{SFR}(M_{\odot} \text{ yr}^{-1}) &= \log L(\text{FUV})_{\text{corr}} - 43.35 \\ \log L(\text{FUV})_{\text{corr}} &= L(\text{FUV})_{\text{obs}} + 3.89L(25 \mu\text{m}) \end{aligned} \quad (1)$$

(Kennicutt & Evans 2012; Hao et al. 2011; Murphy et al. 2011). We obtain FUV magnitudes from the *Galaxy Evolution Explorer* (*GALEX*), and 22 μ m magnitudes from the *Wide-field Infrared Survey Explorer* (*WISE*) (Wright et al. 2010). While the Hao et al. (2011) relation uses 25 μ m luminosities from the *Infrared Astronomical Satellite* (*IRAS*), only three of the galaxies in our sample had *IRAS* detections while all five were detected by *WISE*. Therefore, we use 22 μ m flux densities as a proxy for 25 μ m flux densities as this ratio is expected to be of order unity (Jarrett et al. 2013). The resulting estimates for the SFRs are summarized in Table 5. The SFRs span ~ 0.03 -0.87 $M_{\odot} \text{ yr}^{-1}$, with a median of $\sim 0.27 M_{\odot} \text{ yr}^{-1}$. The uncertainty in this method is ~ 0.13 dex.

The specific star formation rates (sSFR= SFR/M_{\star}) of these BCDs are quite high. Using SFRs calculated above and stellar masses from the NSA, we estimate \log sSFRs in the range -8.6 to -7.9 yr^{-1} . This is comparable to or greater than other dwarf galaxies with AGN candidates such as Mrk 709 and Henize 2-10 (which have \log sSFRs of -8.6 and -9.3 yr^{-1} , respectively; Reines et al. 2014, 2011) and orders of magnitude higher than that of the Large Magellanic Cloud (\log sSFR $\sim -10 \text{ yr}^{-1}$; Whitney et al. 2008; van der Marel et al. 2002).

4.2. Hard X-ray Sources

We search for hard X-ray sources to identify the presence of an accreting BH, compared to star formation which produces high-energy radiation predominantly in the soft X-ray band. To identify hard X-ray sources in our sample of BCDs, we re-run `wavdetect` on (astrometrically corrected) hard images of the S3 chip filtered from 2-7 keV. We adopt wavelet scales of 1.0, 1.4, 2.0, 2.8, 4.0 pixels, a point spread function map describing the 39% enclosed energy fraction at 4 keV, and a significance threshold of 10^{-6} (corresponding to approximately one expected false point source detection across the S3 chip). We then restrict the list of hard X-ray sources identified by `wavdetect` to those that are located within $3r_{50}$ (Petrosian 50% light radii) of the galaxy optical center. How we assess the statistical significance of each hard X-ray source detection is described below.

We extract source counts within circular apertures centered on each source, with aperture radii of 3 pixels ($1''.5$). These apertures correspond to the 90% enclosed energy fraction at 4.5 keV at the S3 aimpoint (all X-ray sources are located < 0.5 from the aimpoint). We adopt these (relatively small) 90% circular apertures to avoid contamination from nearby sources and we visually examine each image to confirm that there is no contamination within any source aperture.

The number of background counts per pixel is estimated by using a circular aperture with 25 arcsec radius centered on a manually selected source-free region of the chip near each galaxy. We consider a source to be detected if the source counts are above the background level within each source aperture at the $>95\%$ confidence level, following the Kraft et al. (1991) Bayesian formalism for Poisson counting statistics in the presence of a background. Only one `wavdetect` source in Haro 3 fails to meet this detection criterion.

Finally, after subtracting the expected number of background counts in each source aperture from the total counts, a 90% aperture correction is applied to calculate the net counts and net count rates from each source. A total of 10 hard X-ray sources are detected in four galaxies (none are found in II Zw 70), and their properties are reported in Table 6. Note that we exclude an additional source (X2 in SBS 0940+544) from further analysis, as it is likely a background quasar. This source is ~ 20 arcsec away from the main body of the galaxy and it appears in

Table 5
Host Galaxy SFRs and Expected Luminosity from XRBs

Galaxy	FUV (mag)	log L(FUV) (erg s ⁻¹)	W22 (mag)	log L(22 μm) (erg s ⁻¹)	SFR _{FUV} (M _⊙ yr ⁻¹)	log sSFR	log L _{2-10 keV} ^{XRB} (erg s ⁻¹)
(1)	(2)	(3)	(4)	(5)	(6)	(7)	(8)
II Zw 70	14.79	42.6	4.92	41.7	0.27	-7.9	39.0
Haro 3	14.30	42.7	2.50	42.6	0.87	-8.1	39.4
Haro 9	13.53	43.0	3.96	42.1	0.69	-8.5	39.4
Mrk 996	16.47	42.0	4.85	41.8	0.15	-8.6	38.8
SBS 0940+544	17.79	41.7	8.07	40.8	0.03	-8.5	38.2

Note. — Column 1: galaxy name. Column 2: FUV AB magnitudes from *GALEX* (through the NSA). Column 3: log FUV luminosities. Column 4: *WISE* magnitudes^a. Column 5: log 22 μm luminosities. Column 6: estimated SFRs from *GALEX* and *WISE* data. Column 7: log specific SFRs (sSFR=SFR/M_{*}) in units of yr⁻¹. Column 8: log total expected 2-10 keV luminosity from high-mass XRBs.

^aSimilarly to the NSA, SBS 0940+544 appears in *WISE* as two sources; the bright central region and the trailing tail region. The values reported here are for both sources, combined.

the Milliquas catalog of Flesch (2015) under object name SDSS J094418.57+541141.4 with a photometric redshift of ~ 1.6 .

The uncertainty of each hard X-ray position is quoted as the radius of the 95% error circle, as determined from Equation 5 of Hong et al. (2005), who ran simulations to determine the positional accuracy of sources detected by *wavdetect* as a function of counts and location on the ACIS detector. Error bars on counts are quoted at the 90% confidence level. For sources with < 10 total counts, errors are calculated following Kraft et al. (1991), which incorporates the number of background counts in each source aperture. If ≥ 10 total counts, then we assume the background is negligible (all source apertures contain < 0.5 background counts), and we adopt the 90% confidence interval from Gehrels (1986).

Unabsorbed hard X-ray fluxes are calculated from 2-10 keV using the Portable, Interactive Multi-Mission Simulator (PIMMS)⁴. We adopt the Galactic column density from the Dickey & Lockman (1990) maps, and we assume a power-law spectral model with photon index $\Gamma = 1.8$, which is typical for low-luminosity AGN (Ho 2008, 2009) and ultraluminous X-ray sources (Swartz et al. 2008). Unabsorbed fluxes and corresponding luminosities are reported in Table 6. We ignore any potential absorption that is intrinsic to the source and/or host dwarf galaxy, hence these fluxes and luminosities should be considered lower limits.

Finally, we determine that there is a low probability of any of the detected hard X-ray sources in Table 6 being a chance alignment of a resolved X-ray source from the cosmic X-ray background. We estimate the minimum 2-10 keV (unabsorbed) flux sensitivity of each observation that corresponds to detecting 3 hard X-ray counts (i.e., the 1-sided 95% confidence limit assuming no background), given the exposure time of each observation and the Galactic column density toward each galaxy (and assuming $\Gamma = 1.8$). The flux sensitivities range from $S_{\min} = 1.4 \times 10^{-15}$ erg s⁻¹ cm⁻² for our five *Chandra* observations. We then use the resolved cosmic X-ray background log $N - \log S$ relation of Moretti et al. (2003) to estimate $N (> S_{\min})$, the cumulative number of 2-10 keV X-ray sources per deg² with a flux $> S_{\min}$. Based on these $N (> S_{\min})$ estimates, the expected number of

background sources to fall within $3r_{50}$ of each galaxy's optical center is small, ranging from 0.01-0.2 for each of the five galaxy targets.

Our observed 2-10 keV X-ray luminosities range from $\log L_{2-10\text{keV}} (\text{erg s}^{-1}) \sim 38 - 39.5$ (Table 6). Most of our X-ray sources lack optical counterparts, with the exceptions of X1 in Haro 9 and X2 in SBS 0940+544. Two of the galaxies in our sample (with archival *Chandra* data) have previously detected X-ray sources. Georgakakis et al. (2011) searched Mrk 996 for indications of an intermediate mass BH using *Chandra* data, finding no conclusive evidence for one. They detected the same X-ray source presented here (X1) with $L_{0.3-10\text{keV}} = 1.2 \times 10^{39}$ erg s⁻¹, about an order of magnitude higher than the 2-10 keV luminosity we report, as well as another less luminous off-nuclear X-ray source (that we did not detect in the hard 2-10 keV band) with $L_{0.3-10\text{keV}} = 1.8 \times 10^{38}$ erg s⁻¹. Prestwich et al. (2013) detected an X-ray source in SBS 0940+544 (X1 in this paper) with $L_{0.3-8\text{keV}} = 1.26 \times 10^{39}$ erg s⁻¹. While we use the same *Chandra* data as Georgakakis et al. (2011) and Prestwich et al. (2013), the reported source luminosities differ due to the different energy ranges considered.

4.2.1. Expected Contribution from X-ray Binaries

The luminosities of our detected X-ray sources ($L_{2-10\text{keV}} \sim 10^{38-39.5}$ erg s⁻¹) are consistent with either massive BHs accreting well below their Eddington luminosity (e.g., a $\sim 10^4 M_{\odot}$ BH with an Eddington ratio of $\sim 10^{-3}$), or stellar-mass BHs (or neutron stars) in XRBs radiating at a significant fraction of their Eddington luminosity. X-ray emission from high-mass XRBs is known to increase as a function of SFR for late-type galaxies (Grimm, H.-J. et al. 2002; Grimm et al. 2003; Gilfanov et al. 2004; Mineo et al. 2012), whereas low-mass XRBs dominate the XRB population in early-type galaxies and scale with stellar mass (Gilfanov 2004; Humphrey & Buote 2008; Lehmer et al. 2010, 2014). As our target galaxies are generally late-type (irregular) and have high SFRs relative to their stellar mass (see Section 4.1), most of the expected X-ray emission will likely be due to high-mass XRBs.

Enhanced X-ray emission relative the expected contribution from XRBs *could* indicate the presence of a massive BH, however this is neither a necessary nor sufficient condition. For example, a highly sub-Eddington massive

⁴ <http://heasarc.gsfc.nasa.gov/docs/software/tools/pimms.html>

Table 6
Hard X-ray Sources

Source ID	R.A. (deg)	Decl. (deg)	p_{err} (arcsec)	Net Counts	N_{bg} Counts	$F_{2-10 \text{ keV}}$ ($10^{-15} \text{ erg s}^{-1} \text{ cm}^{-2}$)	$\log L_{2-10 \text{ keV}}$ (erg s^{-1})
(1)	(2)	(3)	(4)	(5)	(6)	(7)	(8)
Haro 3–X1	161.346025	55.954587	0.34	76.39 ± 14.94	0.12	90.07	39.5
Haro 3–X2	161.341482	55.961223	0.42	$13.11^{+7.69}_{-5.34}$	0.12	15.46	38.7
Haro 3–X3	161.341573	55.959588	0.47	8.65 ± 4.75	0.12	10.20	38.5
Haro 3–X4	161.346679	55.961958	0.49	7.64 ± 4.45	0.12	9.01	38.5
Haro 3–X5	161.354910	55.961723	0.94	4.31 ± 3.46	0.12	5.08	38.2
Haro 9–X1	191.322023	27.125507	0.35	45.49 ± 11.68	0.08	56.59	39.4
Haro 9–X2	191.320506	27.126089	0.39	20.19 ± 8.02	0.08	25.12	39.0
Haro 9–X3	191.320973	27.126501	0.39	19.28 ± 7.86	0.08	23.98	39.0
Mrk 996–X1	21.898420	-6.325036	0.52	6.72 ± 4.51	0.47	2.66	38.1
SBS 0940+544–X1	146.068446	54.192835	0.40	16.58 ± 7.34	0.12	20.69	39.2

Note. — Column 1: hard X-ray source identification. Column 2: right ascension. Column 3: declination. Column 4: 95% positional uncertainty. Column 5: net counts in the 2-7 keV energy range, after applying a 90% aperture correction. Error bars represent 90% confidence intervals. Column 6: number of background counts expected within each source extraction circle (after applying a 90% aperture correction). Column 7: 2-10 keV flux corrected for Galactic absorption. Column 8: log 2-10 keV luminosity corrected for Galactic absorption.

BH would likely not contribute significantly to the cumulative X-ray emission, and enhanced X-ray emission can originate from very luminous stellar-mass XRBs (Brorby et al. 2014).

Nevertheless, we estimate the expected cumulative 2-10 keV luminosity from XRBs in each galaxy using the relation in Lehmer et al. (2010) which accounts for high-mass XRBs:

$$L_{\text{HX}} = \begin{cases} 10^{(39.57 \pm 0.11)} \text{SFR}^{(0.94 \pm 0.15)} & \text{SFR} \lesssim 0.4 M_{\odot} \text{ yr}^{-1} \\ 10^{(39.49 \pm 0.21)} \text{SFR}^{(0.74 \pm 0.12)} & \text{SFR} \gtrsim 0.4 M_{\odot} \text{ yr}^{-1} \end{cases} \quad (2)$$

We use the SFRs derived in Section 4.1 (Table 5). We note that the uncertainty in the SFRs is ~ 0.13 dex (Hao et al. 2011) and the 1σ scatter in the Lehmer et al. (2010) relationship is ~ 0.4 dex. We find the expected 2-10 keV luminosities from XRB emission to be in the range $\sim 10^{38.2-39.4} \text{ erg s}^{-1}$ (see Table 5).

The observed X-ray luminosities for the galaxies (cumulative from point sources) are generally within the 1σ scatter of the Lehmer et al. (2010) relationship, with the exception of SBS 0940+544 which has an X-ray luminosity $\sim 3\sigma$ higher than would be expected from star formation (see Figure 3; note that II Zw 70 is not plotted as it did not have any observed hard X-ray sources). This discrepancy is unlikely to be due to metallicity, as the metallicities of SBS 0940+544 and Mrk 996 are comparable (at most ~ 0.2 dex difference, from the NSA values) and Mrk 996 has slightly *lower* X-ray luminosity than expected. However, a combination of stochastic effects (regarding XRB formation in galaxies) and the relatively low SFR of SBS 0940+544 could explain this unexpectedly high X-ray luminosity.

If the X-ray source in SBS 0940+544 were a massive BH, we would expect corresponding radio emission as predicted using the fundamental plane of BH activity from Merloni et al. (2003). The luminosity of X1 in SBS 0940+544 is $L_{2-10 \text{ keV}} \sim 10^{39.2} \text{ erg s}^{-1}$ (see Table 6). Assuming a BH mass of $\log(M_{\text{BH}}/M_{\odot}) \sim 3.3 \pm 0.6$ (Reines & Volonteri 2015), we would expect a radio luminosity of $L_{5\text{GHz}} \sim 10^{33.4} \text{ erg s}^{-1}$ where the Merloni

et al. (2003) relation has a scatter of ~ 0.9 dex. Given that the expected radio emission is within our detection limits, and we do not detect radio emission from this source, we do not consider a massive BH to be a likely explanation.

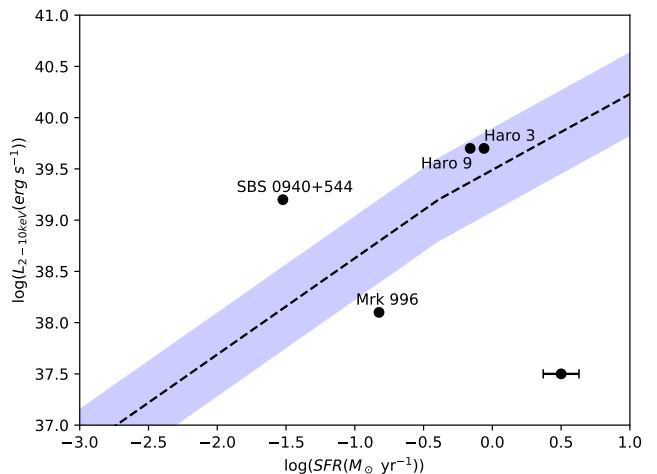


Figure 3. X-ray luminosity vs. SFR for the galaxies. The points represent the observed X-ray luminosities (cumulative from the point sources), while the black dashed line and shaded blue area represent the expected X-ray luminosity and the 1σ scatter using the relation from Lehmer et al. (2010). The uncertainty of ~ 0.13 dex in the SFR is shown in black in the lower right-hand corner. Note that II Zw 70 is absent from this plot as we did not significantly detect any hard X-ray sources.

4.3. Compact Radio Sources

Compact radio emission is detected in all five of our target galaxies (see Figure 2). We use the `detect_sources` and `deblend_sources` functions from the Astropy-affiliated Photutils Python package to select our sources. We use multiples of σ , where σ is the RMS noise (see Table 4) as thresholds for source detection, adapting the threshold to each image as so to eliminate spurious detections. We then relax these thresholds to measure the flux densities to ensure we capture all the emission from the source.

Table 7
Compact Radio Sources

Source ID	R.A.	Decl.	$P_{5\text{GHz}}$	$P_{7.4\text{GHz}}$	$F_{5\text{GHz}}$	$F_{7.4\text{GHz}}$	$\log L_{5\text{GHz}}$	$\log L_{7.4\text{GHz}}$
(1)	(deg)	(deg)	($\mu\text{Jy}/\text{beam}$)	($\mu\text{Jy}/\text{beam}$)	(μJy)	(μJy)	(8)	(9)
II Zw 70–R1	222.735642	35.572258	181	91	360 ± 32	331 ± 33	35.9	36.0
Haro 3–R1	161.344137	55.960794	119	89	93 ± 5	90 ± 5	35.2	35.4
Haro 3–R2	161.343988	55.961128	80	46	77 ± 8	101 ± 12	35.1	35.4
Haro 3–R3a	161.341874	55.961178	725	526	1500 ± 83	1540 ± 86	36.4	36.6
Haro 3–R3b	161.341309	55.960978	664	432	2080 ± 112	2080 ± 113	36.5	36.7
Haro 9–R1	191.321930	27.125492	55	38	24 ± 3	38 ± 3	34.7	35.1
Haro 9–R2	191.321275	27.124692	44	37	45 ± 5	52 ± 10	34.9	35.2
Haro 9–R3	191.320058	27.125258	53	32	39 ± 5	26 ± 4	34.9	34.9
Mrk 996–R1	21.898009	−6.326506	359	230	590 ± 31	549 ± 31	36.2	36.3
SBS 0940+544–R1	146.069071	54.192850	42	24	23 ± 2	19 ± 2	35.0	35.1

Note. — Column 1: radio source identification. Column 2: right ascension. Column 3: declination. Columns 4-5: peak flux values of each source at 5 GHz and 7.4 GHz. Columns 6-7: flux densities (F_ν) at 5 GHz and 7.4 GHz. Columns 8-9: log luminosities (νL_ν) at 5 GHz and 7.4 GHz in units of erg s^{-1} .

While the flux densities have an intrinsic $\sim 5\%$ error due to calibration⁵, we also introduce uncertainty into our measurements via the exact choice of background we use for each source. To account for this, we take multiple measurements of each source, varying said background. We report the average flux densities from these measurements, and include both the intrinsic $\sim 5\%$ error and the standard deviation of these measurements in our reported uncertainties.

We identify a total of 10 compact radio sources across the five galaxies, with luminosities in the range $4.8 \times 10^{34} - 5.2 \times 10^{36} \text{ erg s}^{-1}$. Due to uncertainties in flux densities and limited frequency coverage, we are not able to reliably determine the spectral indices for most of our sample. Two of the galaxies in our sample have previously detected compact radio sources. Cox et al. (2001) combined 1.4 GHz radio and optical observations to analyze the polar ring of II Zw 71, the companion galaxy to II Zw 70; they also detected the radio source we denote as R1 in this work. Johnson et al. (2004) used 8.3 GHz and 23 GHz radio observations to study the ongoing star formation in Haro 3 and detected the same radio sources presented here.

4.3.1. Comparison to Thermal HII Regions and SNRs

While we are primarily interested in detecting potential radio emission from accreting massive BHs, we must also consider alternative origins for the observed compact radio emission since we are dealing with lower luminosities compared to more massive systems. We are mainly concerned about free-free emission from dense HII regions and synchrotron emission from supernova remnants.

We first consider the possibility that the radio emission is entirely thermal and emanating from dense HII regions associated with extragalactic massive star clusters. Under this assumption, we estimate the ionizing flux, Q_{Lyc} ,

of the radio sources following Condon (1992):

$$\left(\frac{Q_{Lyc}}{\text{s}^{-1}}\right) \gtrsim 6.3 \times 10^{52} \left(\frac{T_e}{10^4 \text{ K}}\right)^{-0.45} \left(\frac{\nu}{\text{GHz}}\right)^{0.1} \times \left(\frac{L_{\nu, \text{thermal}}}{10^{27} \text{ erg s}^{-1} \text{ Hz}^{-1}}\right). \quad (3)$$

We assume an electron temperature $T_e \sim 10^4 \text{ K}$ for all sources and use the 7.4 GHz luminosities from Table 7. Adopting $Q_{Lyc} = 10^{49} \text{ s}^{-1}$ as the ionizing flux of a typical O-type main sequence star (O7.5 V star; Vacca et al. 1996), we find ionizing fluxes corresponding to the equivalent of ~ 80 to 5410 O-type stars (median value of 250 O-type stars). The calculated ionizing fluxes are consistent with thermal radio sources associated with young massive star clusters in other star-forming dwarf galaxies (e.g., Johnson et al. 2004; Reines et al. 2008; Aversa et al. 2011; Kepley et al. 2014).

We also calculate the expected galaxy-wide ionizing fluxes using the UV-derived SFRs in Section 4.1 and Equation 2 in Kennicutt (1998), and compare these values to those from adding up the individual radio sources. We find the two to generally be in agreement, differing by at most a factor of ~ 2 with the exception of Haro 9. The UV-derived galaxy-wide ionizing flux of Haro 9 is greater by a factor of ~ 18 compared to the sum of the radio sources. This discrepancy is likely due to the large amount of extended emission in Haro 9 (see Figures 2e, 2f), which is included in the galaxy-wide UV-derived ionizing flux but excluded when simply adding up the ionizing fluxes of the individual sources.

Next we compare the luminosities of our detected radio sources with known radio SNRs. We assume a typical SNR spectral index of $\alpha = 0.7$, where $F_\nu \propto \nu^{-\alpha}$, and convert our 7.4 GHz flux densities (Table 7) to 1.45 GHz spectral luminosities to compare with the SNR spectral luminosities in Chomiuk & Wilcots (2009).

The corresponding 1.45 GHz spectral luminosities span a range of $\sim 2 \times (10^{25} - 10^{27}) \text{ erg s}^{-1} \text{ Hz}^{-1}$, which are consistent with or slightly above the radio SNRs in Chomiuk & Wilcots (2009) ($L_{1.4\text{GHz}} \sim 10^{23} - 10^{27} \text{ erg s}^{-1} \text{ Hz}^{-1}$). We therefore conclude that the compact radio sources in our sample are not so luminous as to exclude star-formation-related emission in the form of HII regions

⁵ <https://science.nrao.edu/facilities/vla/docs/manuals/oss/performance/fdscale>

and/or SNRs.

4.4. A Candidate Low-luminosity AGN in Haro 9

As described above, we have detected 10 hard X-ray point sources and 10 compact radio sources in our sample of five blue compact dwarf galaxies. The luminosities of these sources could be produced by sub-Eddington massive BHs, however the X-ray and radio luminosities alone are also within the expected ranges for stellar processes (see Sections 4.2.1, 4.3.1). We therefore search for spatially coincident X-ray and radio sources (Figure 4), for which the ratio of the luminosities can provide some clues to the origin of the emission.

We find one example of a spatially coincident X-ray and radio source in Haro 9 (X1 and R1 in Figure 4c) within the positional uncertainties. The hard X-ray source has a luminosity of $\log L_{2-10\text{keV}} = 39.4$ and the compact radio source has a luminosity of $\log L_{5\text{GHz}} = 34.7$, where the units are in erg s^{-1} . We make use of the ratio of the radio and X-ray luminosities following Terashima & Wilson (2003),

$$R_X = \frac{\nu L_\nu(5 \text{ GHz})}{L_X(2-10 \text{ keV})}, \quad (4)$$

and find that $\log R_X \sim -4.7$.

We see that the source is too luminous in the radio to be a stellar-mass XRB (e.g., Gallo et al. 2018), which have $\log R_X \lesssim -5.3$. While in principle the radio emission could be due to a radio flare associated with an XRB state transition, with a radio luminosity of $\log L_{5\text{GHz}} \sim 34.7$ the source would be brighter than the brightest flare we have seen from an XRB in our own galaxy (Cyg X-3, $\log L_{15\text{GHz}} \sim 34.3$; Corbel et al. 2012). Additionally, the likelihood of catching a state transition is rare, especially with both the radio and X-ray emission so bright, given that the observations were taken ~ 3 weeks apart (state transitions usually last from a few days to a few weeks; Yu & Yan 2009). As such, the source is unlikely to be a stellar-mass XRB, even one undergoing a state transition.

The X-ray/radio source is also not likely to be a SNR, since these objects are typically much more luminous in the radio with $\log R_X > -2.7$ (see Supplementary Information in Reines et al. 2011, and references therein).

A more reasonable possibility is an ultra-luminous X-ray source (ULX) bubble. This would account for the X-ray luminosity, and the observed radio luminosity does not exceed values for ULX bubbles found in the literature (e.g. Motch et al. 2010; Cseh et al. 2012, with $\log L_R \sim 35.3$). While many ULX bubbles are extended, measuring hundreds of pc across in the optical (Pakull & Mirioni 2002, 2003), bubbles as small as ~ 40 pc have been observed in the radio (Lang et al. 2007), which is consistent with the VLA resolution of our observed point-like source. Thus, if the source is a ULX bubble, it would have to be a luminous and relatively compact one.

The source is also consistent with a low-luminosity AGN. From Figure 3 in Merloni et al. (2003), we see that the source falls within the range of massive black holes in the compact radio luminosity versus hard X-ray luminosity plane. Under the assumption that the source is indeed an accreting massive BH, the fundamental plane of BH activity relating BH mass to radio and X-ray luminosity

implies a BH mass of $\log (M_{\text{BH}}/M_\odot) \sim 4.8 \pm 1.1$ using the Merloni et al. (2003) relation and $\log (M_{\text{BH}}/M_\odot) \sim 5.2 \pm 0.44$ using the Miller-Jones et al. (2012) relation. Using the scaling between BH mass and host galaxy total stellar mass ($\sim 10^{8.38} M_\odot$ for Haro 9; see Table 1) for local AGNs from Reines & Volonteri (2015) provides a BH mass of $\log (M_{\text{BH}}/M_\odot) \sim 4.7 \pm 0.55$. If the source is indeed a massive black hole, it must be accreting at a modest rate given the low X-ray luminosity. Assuming a black hole mass of $M_{\text{BH}} \sim 10^5 M_\odot$ and an X-ray bolometric correction of 20 (Vasudevan & Fabian 2009), the corresponding Eddington fraction would be $\sim 0.4\%$.

We note that the ratios and comparisons discussed above are only valid if the X-ray and radio emission are indeed coming from the same source. The positional offset between X1 and R1 in Haro 9 is $0''.3$. While this is within the positional uncertainties, we cannot definitively say the X-ray and radio emission come from the same object. Moreover, there is a star cluster complex in the same region as the X-ray/radio source(s) that could plausibly host both an XRB and SNR (or H II region). Therefore, we caution that this apparently coincident X-ray/radio source in Haro 9 should be considered a *candidate* low-luminosity AGN.

4.5. Detection Limits

AGNs in dwarf galaxies are powered by less massive BHs than typical AGNs in more massive galaxies (e.g., Reines & Volonteri 2015), and will therefore be less luminous. As an example, the Eddington luminosity of a $10^4 M_\odot$ BH is only $\sim 10^{42} \text{ erg s}^{-1}$. However, we know that BHs with high accretion rates are rare (e.g., Schulze, A. & Wisotzki, L. 2010) so the actual luminosities of AGNs in dwarf galaxies may be orders of magnitude lower. Therefore, we must lower our luminosity threshold for what *could* be an AGN in dwarf galaxy, which we have explored in the preceding sections. We also require sensitive, high-resolution observations in order to probe lower luminosities and isolate compact X-ray/radio emission from that of the host galaxy on larger scales.

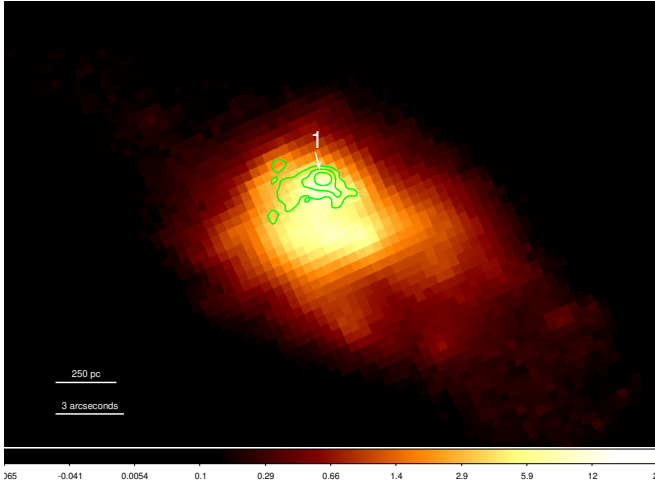
Here we estimate detection limits of potential massive BHs in our sample of BCDs. We first estimate the expected BH masses based on the scaling relation between BH mass and host galaxy total stellar mass for local AGNs in Reines & Volonteri (2015). Given the stellar masses in Table 1, we expect BH masses in the range $\log (M_{\text{BH}}/M_\odot) \sim 3.3 - 4.7$, with a median of $\log (M_{\text{BH}}/M_\odot) \sim 4.0$. The scatter in the Reines & Volonteri (2015) relation is ~ 0.55 dex. Next we use our X-ray detection limits to determine the minimum detectable Eddington fractions of BHs with these masses. The Eddington fraction is given by

$$f_{\text{Edd}} = (\kappa L_X)/(L_{\text{Edd}}) \quad (5)$$

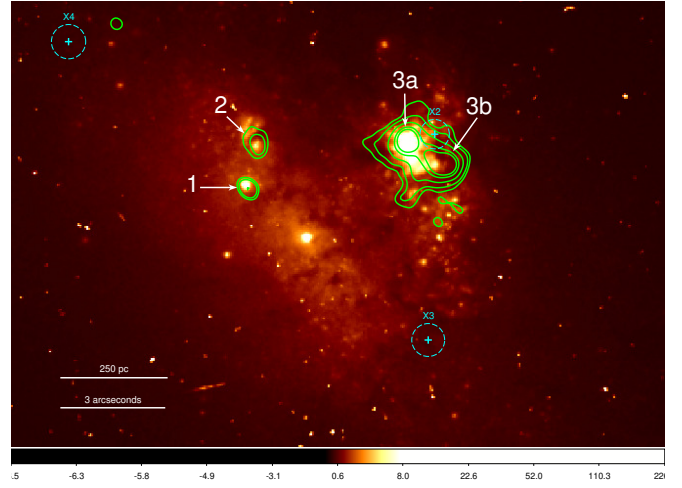
where κ is the 2-10 keV bolometric correction and L_X , L_{Edd} are the X-ray and Eddington luminosity of the BH, respectively. We find L_{Edd} from the BH masses via

$$L_{\text{Edd}} \approx 1.26 \times 10^{38} M_{\text{BH}}/M_\odot \text{ erg s}^{-1} \quad (6)$$

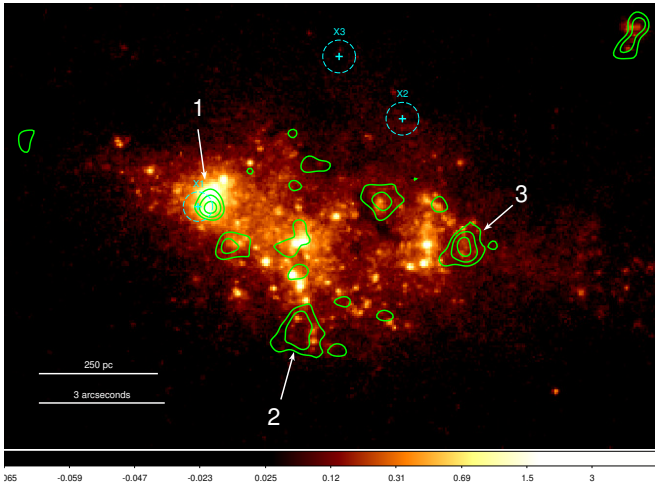
and take $L_X \sim 10^{38} \text{ erg s}^{-1}$, which is the minimum detectable X-ray luminosity corresponding to our X-ray flux sensitivity of $F_X \sim 2.5 \times 10^{-15} \text{ erg s}^{-1} \text{ cm}^{-2}$ (see Section 4.2) at the distances of our galaxies (~ 20 Mpc). We



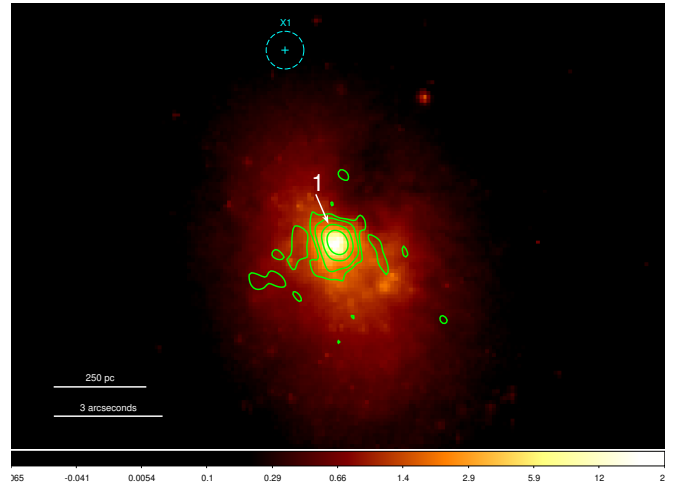
(a) II Zw 70 optical image from the SDSS (*g* band).



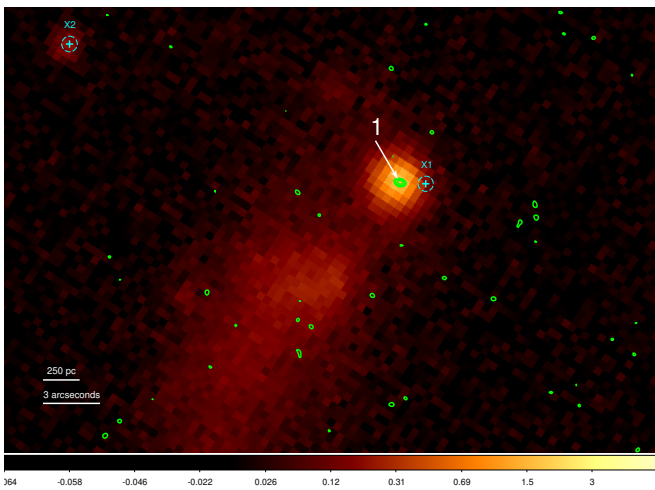
(b) Haro 3 optical image from *HST*/WFPC2 (F606W filter). Note that X-ray sources X1 and X5 are out of view.



(c) Haro 9 optical image from *HST*/WFPC2 (F439W filter).



(d) Mrk 996 optical image from *HST*/WFPC2 (F569W filter).



(e) SBS 0940+544 optical image from the SDSS (*g* band). Note that X-ray source X2 is likely a background quasar (see Section 4.2), and thus is excluded from our analysis.

Figure 4. Optical images from *HST* or the SDSS as indicated, with X-ray sources (cyan) and 5 GHz radio contours (green) overlaid. For the X-ray sources, the cyan crosses and circles mark the position of the source and the 95% positional uncertainty. The only case of spatially coincident X-ray and radio sources within the positional uncertainties is in Haro 9, between X1 and R1.

assume these BHs are accreting at low rates ($f_{\text{Edd}} \lesssim 0.1$) giving $\kappa \sim 15 - 30$ (Vasudevan & Fabian 2009). Adopting $\kappa \sim 30$ (for an upper bound) and $M_{\text{BH}} \sim 10^4 M_{\odot}$, we find $\log f_{\text{Edd}} \sim -2.8$. In other words, our X-ray observations are sensitive enough to detect a $\sim 10^4 M_{\odot}$ BH radiating at $\sim 0.1\%$ of its Eddington luminosity. The corresponding radio luminosity predicted from the fundamental plane of BH activity (Merloni et al. 2003) is $\sim 10^{33} \text{ erg s}^{-1}$, albeit with large uncertainty – the 1σ scatter in the relation is ~ 0.9 dex. Our VLA observations are sensitive to radio luminosities of $\sim \text{a few } \times 10^{34} \text{ erg s}^{-1}$, making this right on the edge of what we could detect (including the ~ 0.9 dex uncertainty).

5. SUMMARY AND CONCLUSIONS

We have presented high-resolution *Chandra* and VLA observations of five low-mass blue compact dwarf galaxies in a search for X-ray and radio signatures of accreting massive BHs. We detected 10 hard X-ray point sources and 10 compact radio sources in our sample, which in all but one case did not overlap. While we were primarily interested in detecting signatures of massive BHs, we considered possible alternative origins for the observed radio and X-ray emission such as thermal HII regions, SNRs, and XRBs. None of the X-ray and radio sources alone were so luminous as to rule out star-formation-related emission.

In the BCD Haro 9, however, we detected a spatially coincident X-ray and radio source (within the astrometric uncertainties) that was consistent with an active massive BH ($M_{\text{BH}} \sim 10^5 M_{\odot}$) under the assumption that the X-ray and radio emission originated from the same source. We cautioned that the combination of a stellar-mass X-ray binary plus a supernova remnant (or H II region) could also account for the X-ray and radio sources, respectively, which are located in the vicinity of a star cluster complex.

Compared to other dwarf galaxies found to host active massive BHs (e.g., Reines et al. 2011, 2013, 2014), our sample of BCDs have significantly lower stellar masses ($\sim 10\times$ on average). Moreover, in contrast to optically-selected samples (e.g., Reines et al. 2013), the BCDs studied here are actively star-forming with somewhat disturbed morphologies. The lack of convincing detections of massive BHs in our sample of BCDs could be suggestive of the BH occupation fraction dropping off with decreasing galaxy mass, or that BHs in BCDs are not commonly accreting at a detectable rate. Indeed, recent simulations indicate that BH growth in low-mass galaxies can be stunted by supernova feedback (e.g., Habouzit et al. 2017; Anglés-Alcázar et al. 2017) and that the conditions for rapid BH accretion in dwarf galaxies are rare (Bellovary et al. 2019).

While this work has broadened the parameter space in the search for massive BHs in dwarf galaxies, future studies with larger sample sizes are necessary to more accurately determine the prevalence of massive BHs in low-mass star-forming dwarfs such as BCDs and help shed light on the origin of BH seeds (e.g., Plotkin & Reines 2018).

We thank the referee for their comments and gratefully acknowledge helpful conversations from Gregory

Sivakoff and Kelsey Johnson during the early stages of this project. Support for this work was provided by NASA through *Chandra* Award Number GO2-13126 issued by the *Chandra X-ray Observatory Center*, which is operated by the Smithsonian Astrophysical Observatory for and on behalf of the NASA under contract NAS8-03060. TDR acknowledges support from the Netherlands Organisation for Scientific Research (NWO) Veni Fellowship. The National Radio Astronomy Observatory is a facility of the National Science Foundation operated under cooperative agreement by Associated Universities, Inc. The scientific results reported in this article are based in part on observations made by the *Chandra X-ray Observatory*. They are also based on observations made with the NASA/ESA Hubble Space Telescope, and obtained from the Hubble Legacy Archive, which is a collaboration between the Space Telescope Science Institute (STScI/NASA), the European Space Agency (ST-ECF/ESAC/ESA) and the Canadian Astronomy Data Centre (CADM/NRC/CSA). Funding for the Sloan Digital Sky Survey IV has been provided by the Alfred P. Sloan Foundation, the U.S. Department of Energy Office of Science, and the Participating Institutions. SDSS acknowledges support and resources from the Center for High-Performance Computing at the University of Utah. The SDSS web site is www.sdss.org. This publication makes use of data products from the Wide-field Infrared Survey Explorer, which is a joint project of the University of California, Los Angeles, and the Jet Propulsion Laboratory/California Institute of Technology, funded by the National Aeronautics and Space Administration. This work has also used observations made with the NASA Galaxy Evolution Explorer. GALEX is operated for NASA by the California Institute of Technology under NASA contract NAS5-98034. Funding for the NASA-Sloan Atlas has been provided by the NASA Astrophysics Data Analysis Program (08-ADP08-0072) and the NSF (AST-1211644).

REFERENCES

- Anglés-Alcázar, D., Faucher-Giguère, C.-A., Quataert, E., et al. 2017, *MNRAS*, 472, L109
- Aversa, A. G., Johnson, K. E., Brogan, C. L., Goss, W. M., & Pisano, D. J. 2011, *The Astronomical Journal*, 141, 125
- Baldassare, V. F., Geha, M., & Greene, J. 2018, *ApJ*, 868, 152
- Baldassare, V. F., Reines, A. E., Gallo, E., & Greene, J. E. 2015, *The Astrophysical Journal Letters*, 809, L14
- . 2017, *The Astrophysical Journal*, 836, 20
- Baldassare, V. F., Reines, A. E., Gallo, E., et al. 2016, *The Astrophysical Journal*, 829, 57
- Becker, R. H., White, R. L., & Helfand, D. J. 1995, *ApJ*, 450, 559
- Bellovary, J. M., Cleary, C. E., Munshi, F., et al. 2019, *MNRAS*, 482, 2913
- Brorby, M., Kaaret, P., & Prestwich, A. 2014, *Monthly Notices of the Royal Astronomical Society*, 441, 2346
- Chomiuk, L., & Wilcots, E. M. 2009, *The Astrophysical Journal*, 703, 370
- Condon, J. J. 1992, *Annual Review of Astronomy and Astrophysics*, 30, 575
- Corbel, S., Dubus, G., Tomsick, J. A., et al. 2012, *Monthly Notices of the Royal Astronomical Society*, 421, 2947
- Cox, A. L., Sparke, L. S., Watson, A. M., & van Moorsel, G. 2001, *The Astronomical Journal*, 121, 692
- Cseh, D., Corbel, S., Kaaret, P., et al. 2012, *The Astrophysical Journal*, 749, 17
- Dickey, C., Geha, M., Wetzel, A., & El-Badry, K. 2019, arXiv e-prints, arXiv:1902.01401
- Dickey, J. M., & Lockman, F. J. 1990, *ARA&A*, 28, 215
- Flesch, E. W. 2015, *Publications of the Astronomical Society of Australia*, 32, e010

- Fruscione, A., McDowell, J. C., Allen, G. E., et al. 2006, in Society of Photo-Optical Instrumentation Engineers (SPIE) Conference Series, Vol. 6270, Society of Photo-Optical Instrumentation Engineers (SPIE) Conference Series, 1
- Gallo, E., Degenaar, N., & van den Eijnden, J. 2018, MNRAS, 478, L132
- Gehrels, N. 1986, ApJ, 303, 336
- Georgakakis, A., Tsamis, Y. G., James, B. L., & Aloisi, A. 2011, Monthly Notices of the Royal Astronomical Society, 413, 1729
- Gil de Paz, A., Madore, B. F., & Pevunova, O. 2003, The Astrophysical Journal Supplement Series, 147, 29
- Gilfanov, M. 2004, Monthly Notices of the Royal Astronomical Society, 349, 146
- Gilfanov, M., Grimm, H.-J., & Sunyaev, R. 2004, Monthly Notices of the Royal Astronomical Society, 347, L57
- Greene, J. E. 2012, Nature Communications, 3, 1304 EP, review Article
- Greene, J. E., & Ho, L. C. 2007, The Astrophysical Journal, 670, 92
- Grimm, H.-J., Gilfanov, M., & Sunyaev, R. 2003, Monthly Notices of the Royal Astronomical Society, 339, 793
- Grimm, H.-J., Gilfanov, M., & Sunyaev, R. 2002, A&A, 391, 923
- Habouzit, M., Volonteri, M., & Dubois, Y. 2017, MNRAS, 468, 3935
- Hainline, K. N., Reines, A. E., Greene, J. E., & Stern, D. 2016, The Astrophysical Journal, 832, 119
- Hao, C.-N., Kennicutt, R. C., Johnson, B. D., et al. 2011, The Astrophysical Journal, 741, 124
- Hebbar, P. R., Heinke, C. O., Sivakoff, G. R., & Shaw, A. W. 2019, Monthly Notices of the Royal Astronomical Society, 485, 5604
- Ho, L. C. 2008, ARA&A, 46, 475
- , 2009, ApJ, 699, 626
- Hong, J., van den Berg, M., Schlegel, E. M., et al. 2005, ApJ, 635, 907
- Humphrey, P. J., & Buote, D. A. 2008, The Astrophysical Journal, 689, 983
- Jarrett, T. H., Masci, F., Tsai, C. W., et al. 2013, The Astronomical Journal, 145, 6
- Johnson, K. E., Indebetouw, R., Watson, C., & Kobulnicky, H. A. 2004, The Astronomical Journal, 128, 610
- Kennicutt, R. C., & Evans, N. J. 2012, Annual Review of Astronomy and Astrophysics, 50, 531
- Kennicutt, Jr., R. C. 1998, ARA&A, 36, 189
- Kepley, A. A., Reines, A. E., Johnson, K. E., & Walker, L. M. 2014, The Astronomical Journal, 147, 43
- Kormendy, J., & Ho, L. C. 2013, Annual Review of Astronomy and Astrophysics, 51, 511
- Kormendy, J., & Richstone, D. 1995, Annual Review of Astronomy and Astrophysics, 33, 581
- Kraft, R. P., Burrows, D. N., & Nousek, J. A. 1991, ApJ, 374, 344
- Lang, C. C., Kaaret, P., Corbel, S., & Mercer, A. 2007, The Astrophysical Journal, 666, 79
- Lehmer, B. D., Alexander, D. M., Bauer, F. E., et al. 2010, The Astrophysical Journal, 724, 559
- Lehmer, B. D., Berkeley, M., Zezas, A., et al. 2014, The Astrophysical Journal, 789, 52
- Lemons, S. M., Reines, A. E., Plotkin, R. M., Gallo, E., & Greene, J. E. 2015, The Astrophysical Journal, 805, 12
- McMullin, J. P., Waters, B., Schiebel, D., Young, W., & Golap, K. 2007, in Astronomical Society of the Pacific Conference Series, Vol. 376, Astronomical Data Analysis Software and Systems XVI, ed. R. A. Shaw, F. Hill, & D. J. Bell, 127
- Merloni, A., Heinz, S., & di Matteo, T. 2003, MNRAS, 345, 1057
- Miller, B. P., Gallo, E., Greene, J. E., et al. 2015, ApJ, 799, 98
- Miller-Jones, J. C. A., Wrobel, J. M., Sivakoff, G. R., et al. 2012, The Astrophysical Journal Letters, 755, L1
- Mineo, S., Gilfanov, M., & Sunyaev, R. 2012, Monthly Notices of the Royal Astronomical Society, 419, 2095
- Moran, E. C., Shahinyan, K., Sugarman, H. R., Vlez, D. O., & Eracleous, M. 2014, The Astronomical Journal, 148, 136
- Moretti, A., Campana, S., Lazzati, D., & Tagliaferri, G. 2003, ApJ, 588, 696
- Motch, C., Broderick, J. W., Pakull, M. W., Corbel, S., & Soria, R. 2010, Monthly Notices of the Royal Astronomical Society, 409, 541
- Murphy, E. J., Condon, J. J., Schinnerer, E., et al. 2011, The Astrophysical Journal, 737, 67
- Nguyen, D. D., Seth, A. C., Neumayer, N., et al. 2019, ApJ, 872, 104
- Pakull, M. W., & Mirioni, L. 2002, arXiv Astrophysics e-prints, astro-ph/0202488
- Pakull, M. W., & Mirioni, L. 2003, in Revista Mexicana de Astronomia y Astrofisica Conference Series, Vol. 15, Revista Mexicana de Astronomia y Astrofisica Conference Series, ed. J. Arthur & W. J. Henney, 197–199
- Pardo, K., Goulding, A. D., Greene, J. E., et al. 2016, The Astrophysical Journal, 831, 203
- Plotkin, R. M., & Reines, A. E. 2018, in Astronomical Society of the Pacific Conference Series, Vol. 517, Science with a Next Generation Very Large Array, ed. E. Murphy, 719
- Prestwich, A. H., Tsantaki, M., Zezas, A., et al. 2013, The Astrophysical Journal, 769, 92
- Reines, A. E., & Deller, A. T. 2012, The Astrophysical Journal Letters, 750, L24
- Reines, A. E., Greene, J. E., & Geha, M. 2013, The Astrophysical Journal, 775, 116
- Reines, A. E., Johnson, K. E., & Goss, W. M. 2008, The Astronomical Journal, 135, 2222
- Reines, A. E., Plotkin, R. M., Russell, T. D., et al. 2014, The Astrophysical Journal Letters, 787, L30
- Reines, A. E., Reynolds, M. T., Miller, J. M., et al. 2016, The Astrophysical Journal Letters, 830, L35
- Reines, A. E., Sivakoff, G. R., Johnson, K. E., & Brogan, C. L. 2011, Nature, 470, 66 EP
- Reines, A. E., & Volonteri, M. 2015, The Astrophysical Journal, 813, 82
- Ricarte, A., & Natarajan, P. 2018, MNRAS, 481, 3278
- Schramm, M., Silverman, J. D., Greene, J. E., et al. 2013, The Astrophysical Journal, 773, 150
- Schulze, A., & Wisotzki, L. 2010, A&A, 516, A87
- Swartz, D. A., Soria, R., & Tennant, A. F. 2008, The Astrophysical Journal, 684, 282
- Terashima, Y., & Wilson, A. S. 2003, The Astrophysical Journal, 583, 145
- Vacca, W. D., Garmany, C. D., & Shull, J. M. 1996, ApJ, 460, 914
- van der Marel, R. P., Alves, D. R., Hardy, E., & Suntzeff, N. B. 2002, The Astronomical Journal, 124, 2639
- Vasudevan, R. V., & Fabian, A. C. 2009, Monthly Notices of the Royal Astronomical Society, 392, 1124
- Volonteri, M. 2010, The Astronomy and Astrophysics Review, 18, 279
- Whitney, B. A., Sewilo, M., Indebetouw, R., et al. 2008, The Astronomical Journal, 136, 18
- Wright, E. L., Eisenhardt, P. R. M., Mainzer, A. K., et al. 2010, AJ, 140, 1868
- Yu, W., & Yan, Z. 2009, The Astrophysical Journal, 701, 1940